2016

Electrodeposition of MoS2 for Charge Storage in Electrochemical Supercapacitors

Daniel Falola
Southern Illinois University Carbondale

Tomasz Wiltowski
Southern Illinois University Carbondale, tomek@siu.edu

Ian Suni
Southern Illinois University Carbondale, isuni@siu.edu

Recommended Citation
Falola, Daniel, Wiltowski, Tomasz and Suni, Ian. "Electrodeposition of MoS2 for Charge Storage in Electrochemical Supercapacitors." *Journal of the Electrochemical Society* 163, No. 9 (Jan 2016): D568-D574. doi:10.1149/2.0011610jes.

Electrodeposition of MoS_2 for Charge Storage in Electrochemical Supercapacitors

Bamidele D. Falola,[a,d] Tomasz Wiltowski,[c] and Ian I. Suni[,a,b,d]*

[a]Department of Mechanical Engineering and Energy Processes

[b]Department of Chemistry and Biochemistry

[c]Advanced Coal and Energy Research Center

[d]Materials Technology Center

Southern Illinois University

Carbondale, IL 62901

Abstract

Mo sulfide thin films were cathodically electrodeposited onto glassy carbon electrodes (GCE) from aqueous electrolytes containing 10 mM $(NH_4)_2MoS_4$ and 0.2 M KCl. Film adhesion was adequate only for electrodes pretreated by potential cycling in 1.0 M HNO_3 and 0.1 M NaF to enhance the surface roughness and partially oxidize the GCE. Previous studies report direct cathodic electrodeposition of MoS_2, but energy dispersive x-ray spectroscopy and x-ray diffraction suggest that the as-deposited film is closer in stoichiometry to MoS_3, which can be converted to MoS_2 by annealing in Ar at 600°C for one hour. The charge storage capability of electrodeposited Mo sulfide films is studied here for the first time in 1.0 M Na_2SO_4 over the thickness range 50 nm to 5 μm, and before and after high temperature annealing. The highest

capacitance is obtained for 50 nm thick MoS_2 films is 330 F/g measured by galvanostatic charge discharge at 0.75 A/g, and 360 F/g measured by cyclic voltammetry at 10 mV/sec. The capacitance per unit mass decreases with increasing film thickness due to reduced electrochemical accessibility. MoS_2 film formed by high temperature annealing in Ar have a charge storage capability about 40x higher than the as-deposited Mo sulfide films.

*Corresponding Author. Phone: 618-453-7922, E-mail address: isuni@siu.edu.

Molybdenum disulfide (MoS_2) is a layered transition metal sulfide that has been extensively studied for applications such as catalysis,[1] solid phase lubrication,[2] two-dimensional transistors,[3] electronic/spintronic devices,[4] materials for intercalation chemistry,[5] and electrodes for lithium ion batteries.[6] The unique properties of MoS_2 arise from its two dimensional structure that is analogous to that of graphene, with strong Mo-S covalent bonds formed within each layer, and weaker van der Waals bonds between adjacent layers.[7,8] MoS_2 thin films have been fabricated predominantly by chemical vapor deposition (CVD),[9,10] mechanical and chemical exfoliation,[11,12] hydrothermal synthesis,[13,14] microwave heating,[15] and solution phase synthesis.[16,17] Cathodic MoS_2 electrodeposition has also been reported both directly from MoS_4^{2-} precursors and from MoO_4^{2-} electrolytes that also contain either thiosulfate or sulfide as the sulfur source.[18-22] Electrodeposition of MoS_2 is typically simpler and more cost-effective than CVD and related methods, which involve complex and expensive vacuum technologies. In addition, electrodeposition yields nm to μm thick films much more rapidly than exfoliation-based methods. Compared to other solution phase methods, electrodeposition provides excellent control of film thickness. Electrodeposition is widely studied for inexpensive scale-up of thin film applications such as photovoltaic devices and electrochemical supercapacitors.[23] On the other hand, electrodeposition at low temperature does not typically yield crystalline or polycrystalline deposits without post-processing.

In electrochemical supercapacitors, thin film metal oxides are often deposited atop high surface area porous carbon electrodes,[24] which may contain activated carbon, carbon fiber-cloth, carbide-derived carbon, carbon aerogel, graphite, graphene, or carbon nanotubes.[25] The metal oxide coating stores charge during electrode polarization by valence change of the metal ion, thus contributing additional pseudocapacitance to the electrostatic double layer capacitance at the electrode-electrolyte interface.[24] For such applications, desirable properties include chemical stability and corrosion resistance, high electrical conductivity, widespread abundance, non-toxicity, and high surface area per unit volume and mass. The most intensively studied metal oxide coatings for supercapacitor applications include RuO_2, MnO_2, and TiO_2.[26-30]

To date, metal sulfides have attracted less attention than metal oxides as pseudo-capacitive electrode materials within electrochemical supercapacitors. However, chalcogenides such as MoS_2 are intriguing for energy storage applications due to their layered structure, which allows for easier transport and insertion of Li^+ within battery electrodes, as well as ion transport during oxidation and reduction of metal oxide thin films.[7,8] However, while MoS_2 within electrochemical supercapacitors has recently been widely studied, these studies have focused not on MoS_2 thin films, but on complex, composite structures of nm to μm dimensions in order to optimize the total interfacial active area, and therefore maximize the capacitance per unit mass.[7,8] Here we report cathodic electrodeposition of MoS_2 atop glassy carbon electrodes, as well as detailed testing of MoS_2 thin film capacitance, both as a function of film thickness and before and after high temperature annealing.

Experimental

Ammonium tetrathiomolybdate [$(NH_4)_2MoS_4$], KCl, and NaF were obtained from Acros Organics. Anhydrous, ACS-grade Na_2SO_4 was obtained from Sigma Aldrich, while concentrated HNO_3 was purchased from Alfa Aesar. Glassy carbon electrodes (GCE) embedded within a Teflon sleeve were purchased from CH Instruments, and glassy carbon plate was purchased from Alfa Aesar. All reagents were used as received.

Prior to MoS_2 electrodeposition, the GCE was hand polished with 1.0, 0.3, and 0.05 μm alumina powders. For most experiments, the GCE was subsequently given an electrochemical pretreatment of potential cycling at room temperature between +1.5 and -0.4 V vs. Ag/AgCl at 50 mV/s for 300 cycles in an electrolyte containing 1 M HNO_3 and 0.1 M NaF, and then rinsed with ultrapure water. This procedure is a slight modification of a previously reported method for corrosion studies of glassy carbon electrodes.[31] This electrochemical pretreatment process was employed here to enhance the surface roughness and partially oxidize the GCE. This pre-treatment process significantly improves film-substrate

adhesion, since electrodeposited Mo sulfide films delaminated during capacitance measurements without this pre-treatment.

Glassy carbon electrode (GCE) and glassy carbon plate, with and without MoS_2 coating, were used as the working electrodes in a virgin Teflon three-electrode electrochemical cell with a Pt counter electrode and an Ag/AgCl reference electrode. The GCE had an active area of 0.092 cm^2, while the glassy carbon plate had an active area of 0.589 cm^2prior to annealing and 0.118 cm^2 after annealing. Since the electrochemical cell had to be dissembled following Mo sulfide electrodeposition, and subsequently reassembled following thin film annealing (described below), a smaller O-ring was employed upon cell reassembly to ensure that only substrate regions with an electrodeposited thin film are exposed to the electrolyte during subsequent studies. Cyclic voltammetry (CV), galvanostatic charge discharge (GCD), and electrochemical impedance spectroscopy (EIS) measurements were performed with a Gamry Instruments Reference 600. EIS measurements over the frequency range 0.01 Hz to 15 kHz employ an AC probe amplitude of 5 mV, and each scan takes about 2.8 min. to acquire.

For some experiments, MoS_2 electrodeposits onto glassy carbon plate were subsequently annealed in Ar at 600°C for 1 h in a Lindberg Blue M tube furnace. These deposits were then analyzed by scanning electron microscopy (SEM) and energy dispersive x-ray spectroscopy (EDX) in a Quanta 450 FEG from FEI Corp, atomic force microscopy in a Nanosurf FlexAFM, and by powder x-ray diffraction (XRD) in a Rigaku MiniFlex II x-ray diffractometer. Film thickness measurements were performed by stylus profilometery.

Results and Discussion

Electrodeposition of Mo sulfide: Figure 1 shows cyclic voltammetry (CV) results for a glassy carbon electrode (GCE) in an electrolyte containing 10 mM $(NH_4)_2MoS_4$ and 0.2 M KCl at pH 6.8. By comparison to a blank CV scan, the cathodic peak at approximately -1.0 V vs. Ag/AgCl

corresponds to electrodeposition of a Mo sulfide species. While the research group of Levy-Clement first reported cathodic electrodeposition of MoS_2 from MoS_4^{2-},[18-20,] they did not report cathodic voltammetry peaks such as that observed in Figure 1. However, cathodic peaks varying from about -400 to -600 mV vs. Ag/AgCl were reported for Mo sulfide electrodeposition during successive voltage sweeps through both cathodic and anodic peaks for aqueous solutions containing MoS_4^{2-} without a supporting electrolyte.[32] In addition, a cathodic peak was reported at about -1.1 V vs. Ag/AgCl in weakly acidic electrolytes without attribution to a specific cathodic reaction.[33] Electrochemical reduction of Mo sulfide from MoS_4^{2-}-containing electrolytes has been attributed to the following reaction:[18-20]

$$MoS_4^{2-} + 4H^+ + 2e^- \rightarrow MoS_2 + 2H_2S \quad (1)$$

However, the results from subsequent annealing and EDX analysis of the MoS_2 thin films, combined with powder x-ray diffraction (XRD), suggest that the species formed at the cathodic peak in Figure 1 is closer in stoichiometry to MoS_3 than to MoS_2. On the other hand, since the precursor contains Mo(VI), the cathodic reaction evident in Figure 1 probably cannot directly deposit MoS_3, which also contains Mo(VI). It is possible that reaction (1) is correct, but subsequent chemical/electrochemical reactions result in additional sulfur incorporation into the deposit.

Modest H_2 evolution is visually observed during cathodic electrodeposition of Mo sulfide. Comparison of the film thickness measured by profilometery and the total charge transferred during potentiostatic deposition suggests the current efficiency for electrodeposition of Mo sulfide is about 62%. Potentiostatic electrodeposition at -1.0 V vs. Ag/AgCl allows growth of Mo sulfide films of varying thickness. Mo sulfide films more than several μm thick contain nm scale cracks. Some Mo sulfide films were grown on glassy carbon plate and subsequently annealed in Ar at 600°C for 1 h. After this annealing process, cracks were no longer visible in thicker MoS_2 films.

Thin Film Characterization: Following the annealing treatment described above, Figure 2 illustrates top-view and cross-sectional SEM images of a MoS_2 thin film that is approximately 5 μm thick atop a glassy carbon electrode. While such measurements are not fully quantitative, EDX results before and after annealing are consistent with recrystallization of MoS_2 during this process. Prior to annealing, the elemental composition varied, but the elemental Mo:S ratio was always close to 1:3. For annealed films, EDX analyses consistently yield an elemental ratio of Mo:S equal to 1:2 to within experimental error. Loss of sulfur during high temperature annealing is consistent with the low boiling point (444.6°C) of elemental sulfur. AFM measurements over a 5x5 μm^2 scan range show that the high temperature annealing process also reduces the rms surface roughness from 231 to 7 nm for a 5 μm thick film.

Powder x-ray diffraction (XRD) yields no peaks for the Mo sulfide film prior to high temperature annealing. On the other hand, annealed Mo sulfide films yield the XRD pattern shown in Figure 3. This exhibits a broad strong (002) peak at approximately 14.5°, consistent with the formation of crystalline MoS_2.[34,35] From the (002) peak width in Figure 3, the grain size is estimated as 4.3 nm from the Scherrer equation. However, higher peaks that could distinguish between the 2H and 3R polytypes are not observed. Taken together, the EDX and XRD results suggest that the cathodic peak at -1.0 V does not correspond directly to the reaction given in Equation 1, since stoichiometric MoS_2 is only formed after high temperature annealing and loss of a significant amount of sulfur.

Capacitance Testing: As noted above, the research group of Levy-Clement previously reported cathodic electrodeposition of MoS_2 from MoS_4^{2-},[18-20] but to the best of our knowledge, nobody has studied the charge storage capability of electrodeposited MoS_2 thin films. The charge storage capability of Mo sulfide thin films was assessed, before and after high temperature annealing, as a function of film thickness by cyclic voltammetry and galvanostatic charge discharge measurements. During measurements on glassy carbon electrodes (GCE) prepared by mechanical polishing only, the Mo sulfide films delaminated quickly, resulting in a low capacitance value of about 500 $\mu F/cm^2$ after 100 scans. Delamination occurs due to the poor adhesion between the Mo sulfide thin films and the GCE. Therefore

158 subsequent electrodeposition experiments were preceded by potential cycling between +1.5 and -0.4 V vs.
159 Ag/AgCl for 300 cycles at room temperature in an electrolyte containing 1 M HNO_3 and 0.1 M NaF in
160 order to electrochemically roughen and partially oxidize the surface of the GCE, as described above.
161 To demonstrate the potential applications of electrodeposited Mo sulfide thin films as
162 supercapacitor electrodes, its electrochemical performance was investigated by cyclic
163 voltammetry (CV) in 1.0 M Na_2SO_4 at pH 5.1. Figure 4 illustrates the CV curves for 1.0 μm
164 thick as-deposited MoS_3 and three thicknesses of annealed MoS_2 films at different scan rates
165 ranging from 5 to 100 mV/s over the potential range -200 to +400 mV vs. Ag/AgCl reference
166 electrode. The results in Figure 4 exhibit no cathodic or anodic current peaks, so the Mo sulfide
167 films studied here are close to ideal pseudocapacitive materials, albeit over a modest potential
168 window of ~600 mV.[36] From these cyclic voltammograms, the capacitance (C) per unit mass
169 (m) can be determined according to:
170
171 $$C = \frac{S}{2mk\left(U_2 - U_1\right)} \quad (2)$$
172
173 where S is the area enclosed by each curve, k is the scan rate, and U_2 - U_1 is the potential range scanned.
174 The capacitance per unit area (A) can also be obtained from Equation (2) by replacing mass with area.
175 Although studies of thin film metal capacitors often report the capacitance per unit mass, capacitance per
176 unit area is a more fundamental measure of charge storage capability. Such comparisons allow
177 quantitative determination of the value of extra MoS_2 film thickness for increasing the electrode
178 capacitance. One might expect thin film pseudo-capacitance to be limited to only a thin film region near
179 the electrode surface due to transport limitations for ion penetration into the bulk electrode material.
180 Comparing Figures 4a and 4c, the specific capacitance of the as-deposited MoS_3 is about 40x
181 lower than that of the annealed MoS_2 films, so further analysis was performed only on the latter. The low
182 capacitance of the as-deposited film is consistent with deposition of an amorphous film of non-

183 stoichiometric Mo sulfide. The improved film pseudocapacitance after annealing can be attributed to the
184 layered chalcogenide structure, where the relatively weak interlayer bonding provides mechanical
185 flexibility to accommodate ion transport during electrochemical reactions.[7,8]

186 Figure 5 summarizes the results for capacitance testing over 1000 cycles of MoS_2 films from 50
187 nm to 5 μm thick in 1.0 M Na_2SO_4 at a scan rate of 10 mV/sec. As the film thickness increases from 50
188 nm to 5 μm, the capacitance per unit mass in Figure 5 decreases continuously. This is consistent with
189 previous studies of transition metal oxide pseudocapacitance that suggest a penetration depth of 20-50 nm
190 for protons and other species involved in charge storage.[37-39] Material further below the solid-electrolyte
191 interface becomes electrochemically inaccessible, and this is thus at least partly inactive for charge
192 storage. This suggests that the best capacitance obtained here (350-400 F/g at 10 mV/sec) for 50 nm thick
193 MoS_2 cannot be increased much further by electrodeposition of thinner films. Figure 5 illustrates that
194 after 1000 cycles, 50 nm MoS_2 films retain 87% of their original capacitance, and films 250 nm and
195 thicker films retain 90-100% of their original capacitance. Figure 6 illustrates the effect of scan rate on
196 the measured capacitance for a range of MoS_2 film thickness. The decrease in film capacitance with
197 increasing scan rate is often observed for MoS_2 and other materials tested within electrochemical
198 supercapacitors,[40-42] and is expected for the current study due to the relatively thick (μm range) films
199 tested. However MoS_2 electrodes thicker than 50 nm demonstrate excellent capacitance performance at
200 high scan rate. For instance, the specific capacitance, as shown in Figure 6, of 125 nm thick MoS_2
201 electrode at scan rate of 100 mV/s is about 80% comparing with that at 10 mV/s, and this percentage
202 increases with film thickness.

203 MoS_2 film capacitance was also determined by galvanostatic charge discharge (GCD)
204 measurements, with Figure 7 illustrating the GCD results for three different MoS_2 film thickness: 50 nm,
205 1 μm, and 5 μm. The GCD curves are close to the triangular shape expected for ideal pseudocapacitive
206 behavior, except for the lowest current densities studied.[43,44] The capacitance can be precisely
207 determined from the GCD curves using the equation:[45]
208

209 $$C = \frac{i}{m\frac{dU}{dt}} \quad (3)$$

210

211 where i is the discharge current and dU/dt is the derivative of the discharge curve.

212 Figure 8 illustrates the effect of charge/discharge current density on the MoS_2 film capacitance
213 calculated from GCD measurements. The decline in film capacitance with increasing current density in
214 Figure 8 reflects the same underlying phenomena as the decline in capacitance with increasing scan rate
215 in Figure 6, reduced energy storage capability for high power applications. Similar to what is observed
216 for specific capacitance vs. scan rate in Figure 6, MoS_2 electrodes thicker than 50 nm demonstrate good
217 capacitance performance at high current density. Specifically, the specific capacitance of 125 nm thick
218 MoS_2 electrode at current density of 5 A/g is about 80% comparing with that at 1 A/ g. Figure 9
219 summarizes the capacitance measurements obtained for MoS_2 films of different thickness by
220 galvanostatic charge discharge. Figure 9 illustrates that capacitance retention ranges from 74-91% for the
221 different MoS_2 film thickness studied. The current densities at which each curve is given in Figure 9 are
222 chosen for a close correspondence to Figure 5a.

223 The highest capacitance per unit mass obtained for annealed MoS_2 is observed for 50 nm thick
224 films, and ranges from 350-400 F/g from both cyclic voltammetry at 10 mV/sec (Figure 5a) and
225 galvanostatic charge discharge at 0.75 A/g (Figure 9). These values can be compared to other reports of
226 MoS_2 incorporation into electrochemical supercapacitors, but often the materials tested do not correspond
227 to bulk MoS_2 films such as those electrodeposited here, so these comparison must be carefully made. For
228 example, many capacitance measurements on pure MoS_2 involves materials with only 1-3 monolayers
229 thick, whose electronic properties differ substantially from those of bulk MoS_2. In addition, many
230 researchers have studied composite materials that are not purely MoS_2, and their results depend on
231 composition, structure, grain size, and porosity, as well as scan or charging rate.

232 The authors are aware of only three studies of the capacitance of relatively thick, purely MoS_2
233 thin films.[40-42] Hydrothermal synthesis of porous MoS_2 thin films has been reported with capacitance up

234 to 403 F/g.[39] Magnetron sputtering has been employed to grow porous MoS_2 films of capacitance 330
235 F/cm^3.[41] In addition, MoS_2 and graphene nanofilms were grown separately by exfoliation, and then
236 combined into thin film geometry by co-precipitation, yielding film capacitance values as high as 13
237 mF/cm^2.[42] In summary, the best capacitance values obtained here (350-400 F/g) for 50 nm MoS_2 films
238 are similar to the results from references #40-42 for relatively thick MoS_2 films. Higher capacitance
239 values ranging from 416-589 F/g have been reported for MoS_2 nanocomposites with reduced graphene
240 oxide,[43] carbon nanotubes,[46] porous carbon,[47] polyaniline,[48] and WS_2 and amorphous carbon.[49] In
241 addition, much higher capacitance values up to 1544 F/g have been reported for MoS_2-Ni_2S_3
242 nanocomposites atop porous C and Ni electrodes.[50,51]

243 The nature and stability of annealed MoS_2 thin films of different thickness were further
244 investigated by electrochemical impedance spectroscopy (EIS) in 1.0 M Na_2SO_4. EIS studies are
245 sometimes employed to verify that materials intended for charge storage within electrochemical
246 supercapacitors are truly pseudocapacitive, and thus can be charged and discharged rapidly.[36] The results
247 for a 1.0 μm thick annealed MoS_2 film, before and after capacitance testing by cyclic voltammetry , are
248 shown in Figure 10. In these Nyquist plots, the real component of the impedance is plotted on the x-axis
249 and the imaginary component on the y-axis. For materials that undergo redox reactions, the Nyquist plot
250 exhibits a semicircular shape at intermediate to high frequencies, indicating relatively slow charge
251 transfer. The results in Figure 10 are consistent with truly pseudocapacitive materials, with the expected
252 capacitive behavior approaching a vertical line.[43] The results for other MoS_2 film thickness are almost
253 identical.

254 In addition, the results of Figure 10 suggest that the electrical properties of the MoS_2 thin film are
255 largely unaffected by capacitance testing. However, the slight reduction in the x-intercept likely indicates
256 that the MoS_2 film resistance decreases slightly during capacitance testing. Although the difference in the
257 x-intercepts is small, this is a real affect, since the electrochemical cell was not disturbed during these
258 measurements, so the electrode positions remain fixed.
259

Conclusions

Mo sulfide thin films can be cathodically electrodeposited onto glassy carbon from aqueous electrolytes containing 10 mM $(NH_4)_2MoS_4$ and 0.2 M KCl at pH 6.8. EDX measurements yield a Mo:S elemental ratio of about 1:3 in the as-deposited films, but this changes to 1:2 after annealing at 600°C in Ar for one h. Similarly, the as-deposited Mo sulfide films do not exhibit any XRD peaks, but a broad MoS_2 (002) peak is observed after high temperature annealing. From the Scherrer equation, the grain size is estimated as 4.3 nm. For the first time, the charge storage capability of electrodeposited Mo sulfide films is studied by potential scanning and galvanostatic charge discharge measurements in 1.0 M Na_2SO_4 over the thickness range 50 nm to 5 μm. The highest capacitance obtained ranges from 350-400 F/g for 50 nm thick MoS_2 films. MoS_2 film formed by high temperature annealing in Ar have a charge storage capability about 40x higher than the as-deposited Mo sulfide films.

References

1. E.G. Firmiano, M.A. Cordeiro, A.C. Rabelo, C.J. Dalmaschio, A.N. Pinheiro, E.C. Pereira, and R. Leite, *Chem. Commun*., **48**, 7687 (2012).
2. J.R. Lince, *Trib. Lett*., **17**, 419 (2004).
3. B. Radisavljevic, A. Radenovic, J. Brivio, V. Giacometti, and A. Kis, *Nat. Nanotech*., **6**, 147 (2011).
4. A. Dankert, L. Langouche, M.V. Kamalakar, and S.P. Dash, *ACS Nano*, **8**, 476 (2014).
5. E. Benavente, M. Santa Ana, F. Mendizábal, and G. González, G., *Coord. Chem. Rev*., **224**, 87 (2002).
6. K. Chang and W. Chen, *ACS Nano*, **5**, 4720 (2011).
7. X. Rui, H. Tan, and Q. Yan, *Nanoscale*, **6**, 9889 (2014).
8. M. Pumera, Z. Sofer, and A. Ambrosi, *J. Mater. Chem. A*, **2**, 8981 (2014).
9. A. Yan, J. Velasco, S. Kahn, K. Watanabe, T. Taniguchi, F. Wang, M.F. Crommie, and A. Zettl, *Nano Lett*., **15**, 6324 (2015).
10. Y.H. Lee, X.Q. Zhang, W. Zhang, M.T. Chang, C.T. Lin, K.D. Chang, Y.C. Yu, J.T.W. Wang, C.S. Chang, and L.J. Li, *Adv, Mater*., **24**, 2320 (2012).
11. K.G. Zhou, M.N. Mao, H.X. Wang, Y. Peng, and H.L. Zhang, *Angew. Chem. Inter. Ed*., **50**, 10839 (2011).
12. M.B. Sadan, L. Houben, A.N. Enyashin, G. Seifert, and R. Tenne, *Proc. Nat. Acad. Sci*., **105**, 15643 (2008).
13. X. Zhou, B. Xu, Z. Lin, D. Shu, and L. Ma, *J. Nanosci. Nanotechnol.*, **14**, 7250 (2014).
14. D. Kong, H. Wang, J.J. Cha, M. Pasta, K.J. Koski, J. Yao, and Y. Cui, *Nano Lett*., **13**, 1341 (2013).
15. E.G. da Silveira Firmiano, A.C. Rabelo, C.J. Dalmaschio, A.N. Pinheiro, E.C. Pereira, W.H. Schreiner, and E.R. Leite, *Adv, Energy Mater*., **4**, 1301380 (2014).
16. C. Altavilla, M. Sarno, and P. Ciambelli, *Chem. Mater*., **23**, 3879 (2011).

17. K. Chang and W. Chen, *Chem. Commun*., **47**, 4252 (2011).
18. E.A. Ponomarev, M. Neumann-Spallart, G. Hodes, and C. Levy-Clement, *Thin Solid Films*, **280**, 86 (1996).
19. A. Albu-Yaron, C. Levy-Clement, and J. L. Hutchison, *Electrochem. Solid-State Lett*., **2**, 627 (1999).
20. A. Albu-Yaron, C. Levy-Clement, A. Katty, S. Bastide, and R. Tenne, *Thin Solid Films*, **361-362**, 223 (2000).
21. S.K. Ghosh, T. Bera, O. Karacasu, A. Swarnakar, J.G. Buijnsters, and J.P. Celis, *Electrochim. Acta*, **56**, 2433 (2011).
22. S. Shariza and T.J.S. Anand, *Chalcogen. Lett*., **8**, 529 (2011).
23. J. P. Nicholson, *J. Electrochem. Soc.*, **152**, C795 (2005).
24. Patrice Simon and Yury Gogotsi, *Nat. Mater*. **7**, 845 (2008).
25. Marta Sevilla and Robert Mokaya, *Energy Environ. Sci*. **7**, 1250 (2014).
26. B.E. Conway, *Electrochemical Supercapacitors: Scientific Fundamentals and Technological Applications* (Springer Science and Business Media, New York, 2013).
27. J. Miller and B. Dunn, *Langmuir*, **15**, 799 (1999).
28. J.W. Long, K.E. Swider, C.I. Merzbacher, and D.R. Rolison, *Langmuir*, **15**, 780 (1999).
29. J. Miller, B. Dunn, T. Tran, and R Pekala, *J. Electrochem, Soc*,, **144**, L309 (1997).
30. B. Conway, V. Birss, and J. Wojtowicz, *J. Power Sources*, **66**, 1 (1997).
31. G.M. Swain, *J. Electrochem Soc.*, ***141***, 3382 (1994).
32. D. Merki, S. Fierro, H. Vrubel, and X.L. Hu, *Chem. Sci*., **2**, 1262 (2011).
33. J.F. You, D.X. Wu, and H.Q. Liu, *Polyhydron*, **5**, 535 (1986).
34. A.S. Goloveshkin, I.S. Bushmarinov, N.D. Lenenko, M.I. Buzin, A.S. Golub, and M. Yu. Antipin, *J. Phys. Chem. C*, **117**, 8509 (2013).
35. A. N. Enyashin and A. L. Ivanovskii, *J. Struct. Chem*., **54**, 388 (2013).
36. T. Brousse, D. Belanger, and J.W. Long, *J. Electrochem. Soc.*, **162**, A5185 (2015).
37. C.C. Hu, K.H. Chang, M.C. Lin, and Y.T. Wu, *Nano Lett*., **6**, 2690 (2006).

38. Q. Lu, Z.J. Mellinger, W.G. Wang, W.F. Li, Y.P. Chen, J.G. Chen, and J.Q. Xiao, *ChemSusChem*, **3**, 1367 (2011).

39. Z.Y. Lu, Q. Yang, W. Zhu, Z. Chang, J.F. Liu, X.M. Sun, D.G. Evans, and X. Duan, *Nano Res*., **5**, 369 (2012).

40. A. Ramadoss, T.H. Kim, G.S. Kim, and S.J. Kim, *New J. Chem*., **38**, 2379 (2014).

41. N. Choudhary, M. Patel, Y.H. Ho, N.B. Dahotre, W.K. Lee, J.Y. Hwang, and W.B. Choi, *J. Mater. Chem. A*, **3**, 24029 (2015).

42. M.A. Bissett, I.A. Kinloch, and R.A. W. Dryfe, *ACS Appl. Mater. Interf*., **7**, 17388 (2015).

43. K. Gopalakrishnan, K. Pramoda, U. Maitra, U. Mahima, M. A. Shah, and C.N.R. Rao, *Nanomater. Energy*, **4**, 9 (2015).

44. R. Thangappan, S. Kalaiselvam, A. Elayaperumal, R. Jayavel, M. Arivanandhan, R. Karthikey, and Y. Hayakawa, *Dalton Trans*. **45**, 2637 (2016).

45. Meryl D. Stoller and Rodney S. Ruoff, *Energy Environ. Sci*., **3**, 1294 (2010).

46. K.J. Huang, L. Wang, J.Z. Zhang, L.L. Wang, and Y.P. Mo, *Energy*, **67**, 234 (2014).

47. H.M. Ji , C. Liu , T. Wang , J. Chen , Z.M. Mao , J. Zhao , W.H. Hou , and G. Yang, *Small*, **11**, 6480 (2015).

48. J.Y. Lei, Z.Q. Jiang, X.F. Lu, G.D. Nie, and C. Wang, *Electrochim. Acta*, **176**, 149 (2015).

49. J. Xu, L.J. Dong, C.S. Li, and H. Tang, *Mater. Lett*., **162**, 126 (2016).

50. J. Wanga, D.L. Chao, J.L. Liu, L.L. Li, L.F. Lai, J.Y. Lin, and Z.X. Shen, *Nano Energy*, **7**,151 (2014).

51. L.Q. Li, H.B. Yang, J. Yang, L.P. Zhang, J.W. Miao, Y.F. Zhang, C.C. Sun, W. Huang, X.C. Dong, and B. Liu, *J. Mater. Chem. A*, **4**, 1319 (2016).

Figure captions

Figure 1. Cyclic voltammetry of a glassy carbon electrode (GCE) at 30 mV/sec with and without 10 mM $(NH_4)_2MoS_4$ in 0.2 M KCl at pH 6.8.

Figure 2. Top view (a) and cross-sectional (b) SEM images of 5 μm thick MoS_2 thin films atop glassy carbon plate after annealing at 600°C in Ar for 1 h.

Figure 3. Powder x-ray diffraction of MoS_2 thin films scraped off glassy carbon plate after annealing at 600°C in Ar for 1 h.

Figure 4. Cyclic voltammetry curves at different scan rates in 1.0 M Na_2SO_4 for 1 μm as-deposited film (a); and 50 nm (b), 1 μm (c) and 5 μm (d) annealed MoS_2 thin film atop glassy carbon plate.

Figure 5. Capacitance measurements from cyclic voltammetry at 10 mV/s scan rate for different thickness of annealed MoS_2 thin films in units of F/g (a) and F/cm^2 (b) during 1000 cycles in 1.0 M Na_2SO_4.

Figure 6. Specific capacitance measured for first cycle as a function of scan rate and film thickness for annealed MoS_2 films.

Figure 7. Galvanostatic charge/discharge curves of 50 nm (a), 1μm (b) and 5 μm (c) annealed MoS_2 films at different charge/discharge current densities.

Figure 8. Effect of charge/discharge current density on the specific capacitance obtained for different MoS_2 film thickness.

Figure 9. Capacitance measurements from galvanostatic charge/discharge technique for different thickness of MoS_2 thin films during 1000 cycles in 1.0 M Na_2SO_4.

Figure 10. Nyquist plot of EIS results in 1.0 M Na_2SO_4 for MoS_2 film atop glassy carbon plate, before and after capacitance testing.

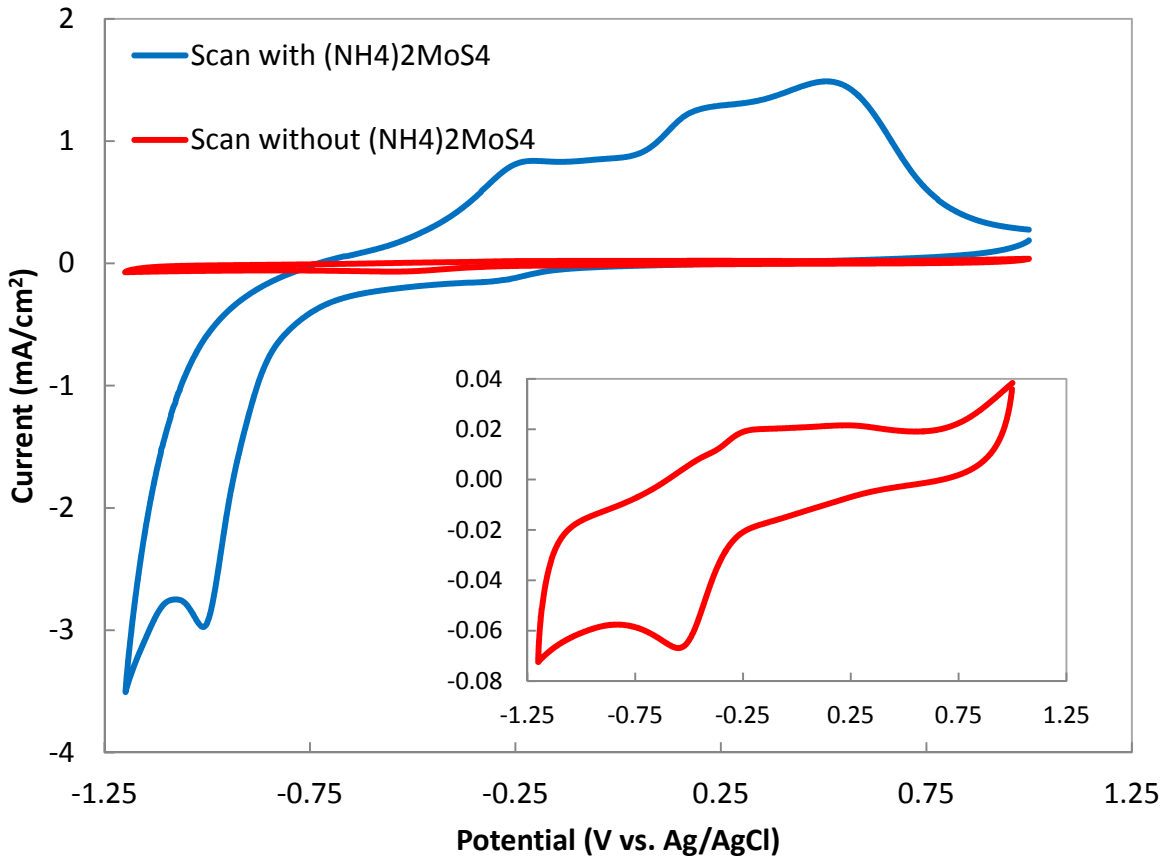
Scan with (NH4)2MoS4
Scan without (NH4)2MoS4
Current (mA/cm²)
Potential (V vs. Ag/AgCl)
2
1
0
-1
-2
-3
-4
-1.25
-0.75
-0.25
0.25
0.75
1.25
0.04
0.02
0.00
-0.02
-0.04
-0.06
-0.08

Figure 1.

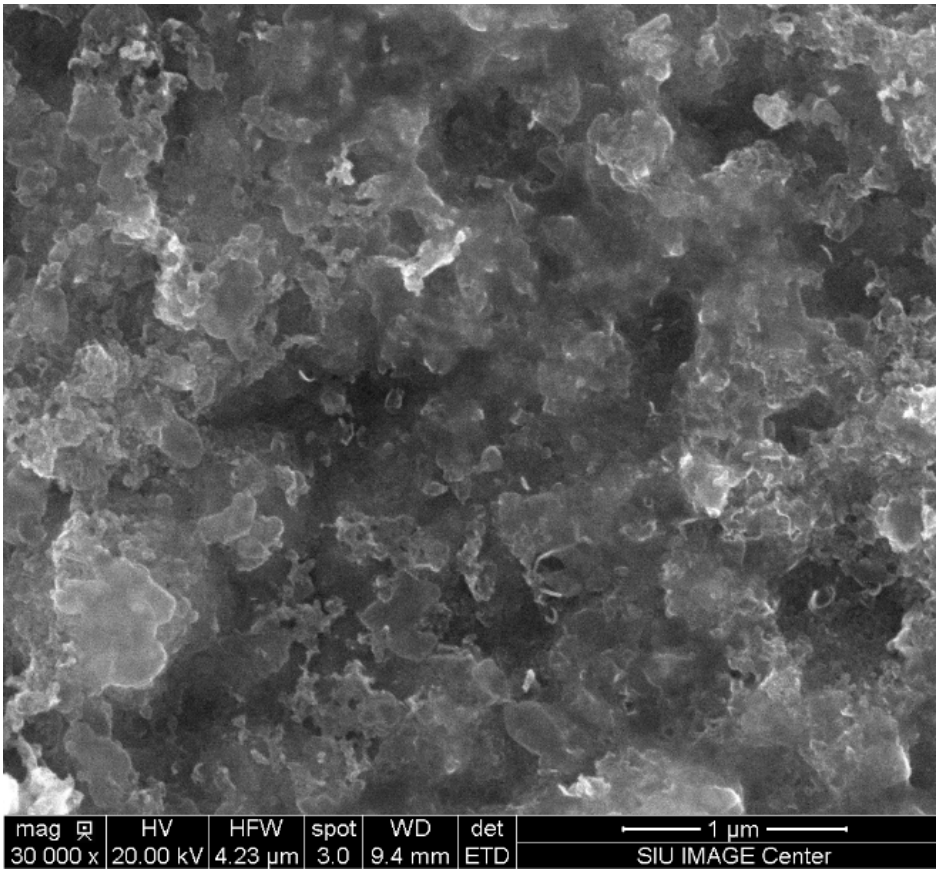
mag
30 000 x
HV
20.00 kV
HFW
4.23 µm
spot
3.0
WD
9.4 mm
det
ETD
1 µm
SIU IMAGE Center

Figure 2a.

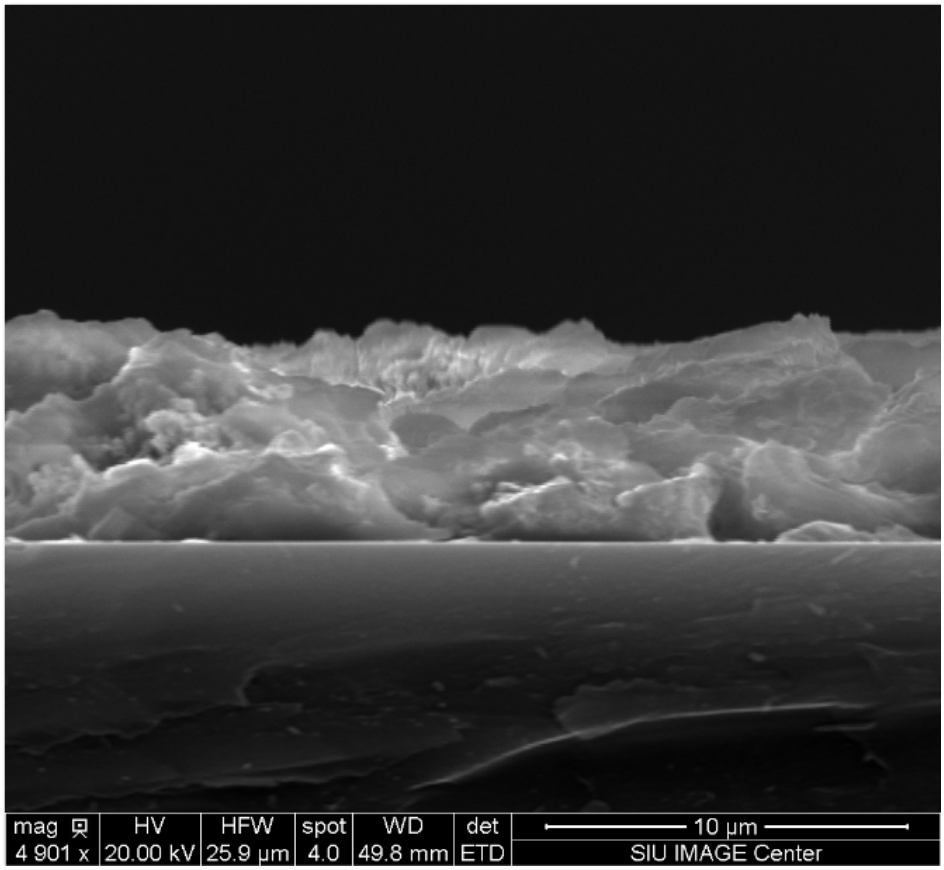
mag
4 901 x
HV
20.00 kV
HFW
25.9 µm
spot
4.0
WD
49.8 mm
det
ETD
10 µm
SIU IMAGE Center

Figure 2b.

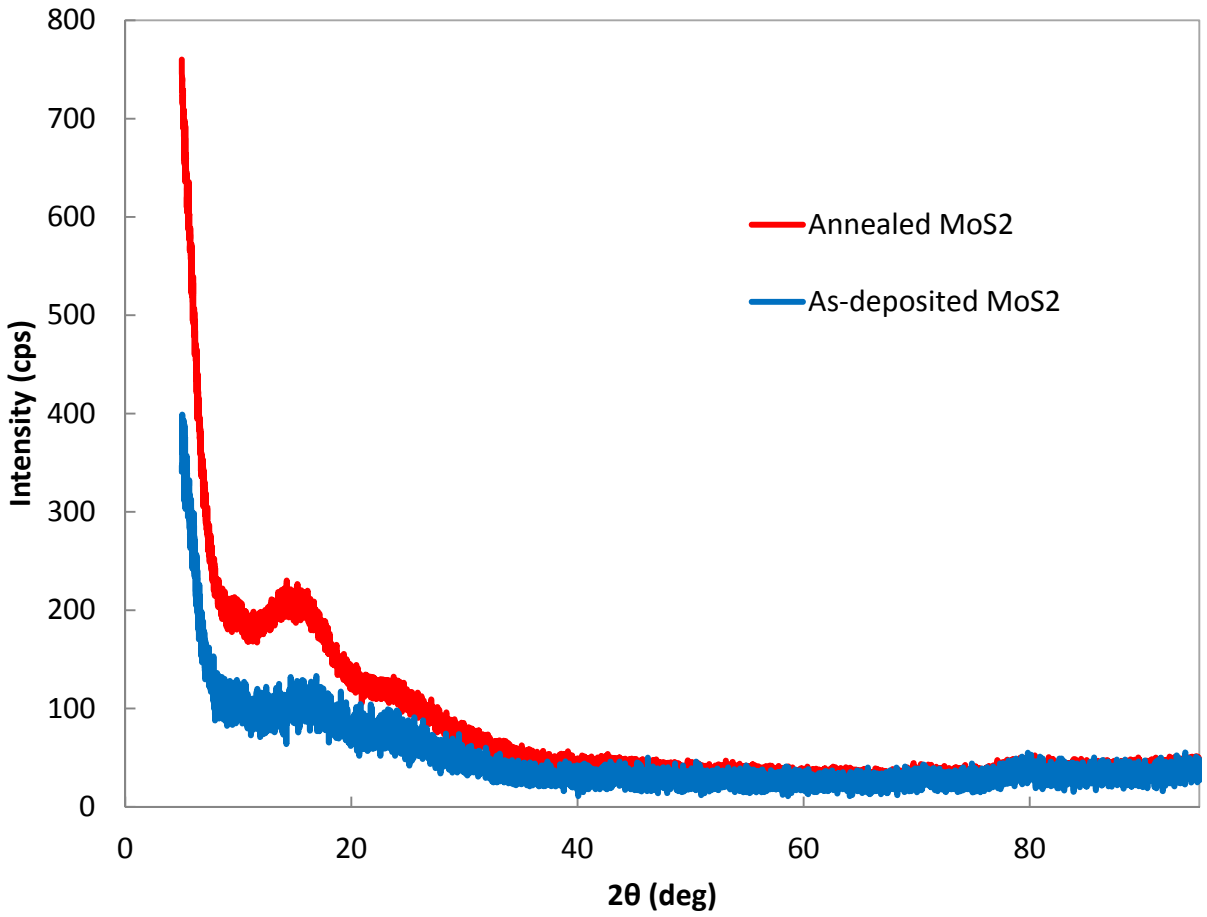
800
700
600
500
400
300
200
100
0
Intensity (cps)
0
20
40
60
80
2θ (deg)
Annealed MoS2
As-deposited MoS2

Figure 3.

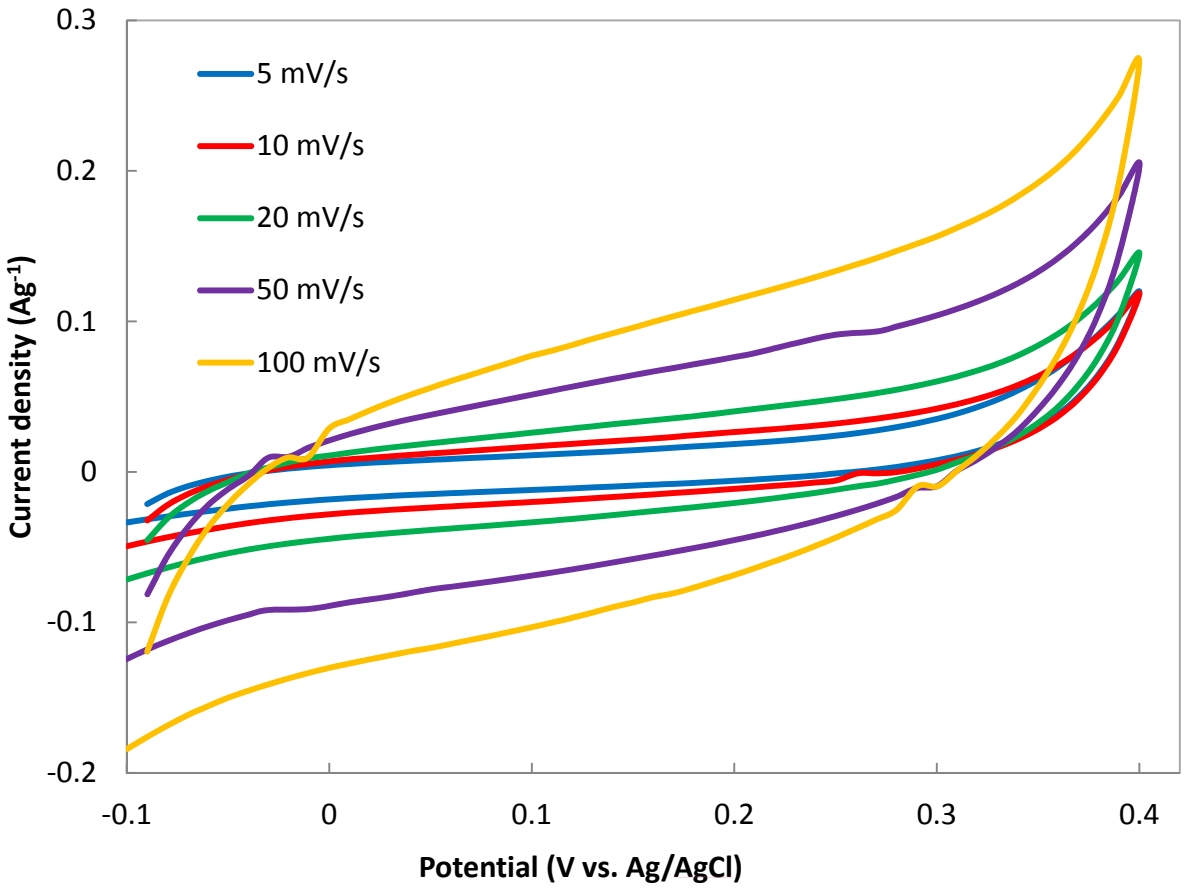
0.3
0.2
0.1
0
-0.1
-0.2
-0.1
0
0.1
0.2
0.3
0.4
5 mV/s
10 mV/s
20 mV/s
50 mV/s
100 mV/s
Current density (Ag-1)
Potential (V vs. Ag/AgCl)

Figure 4a.

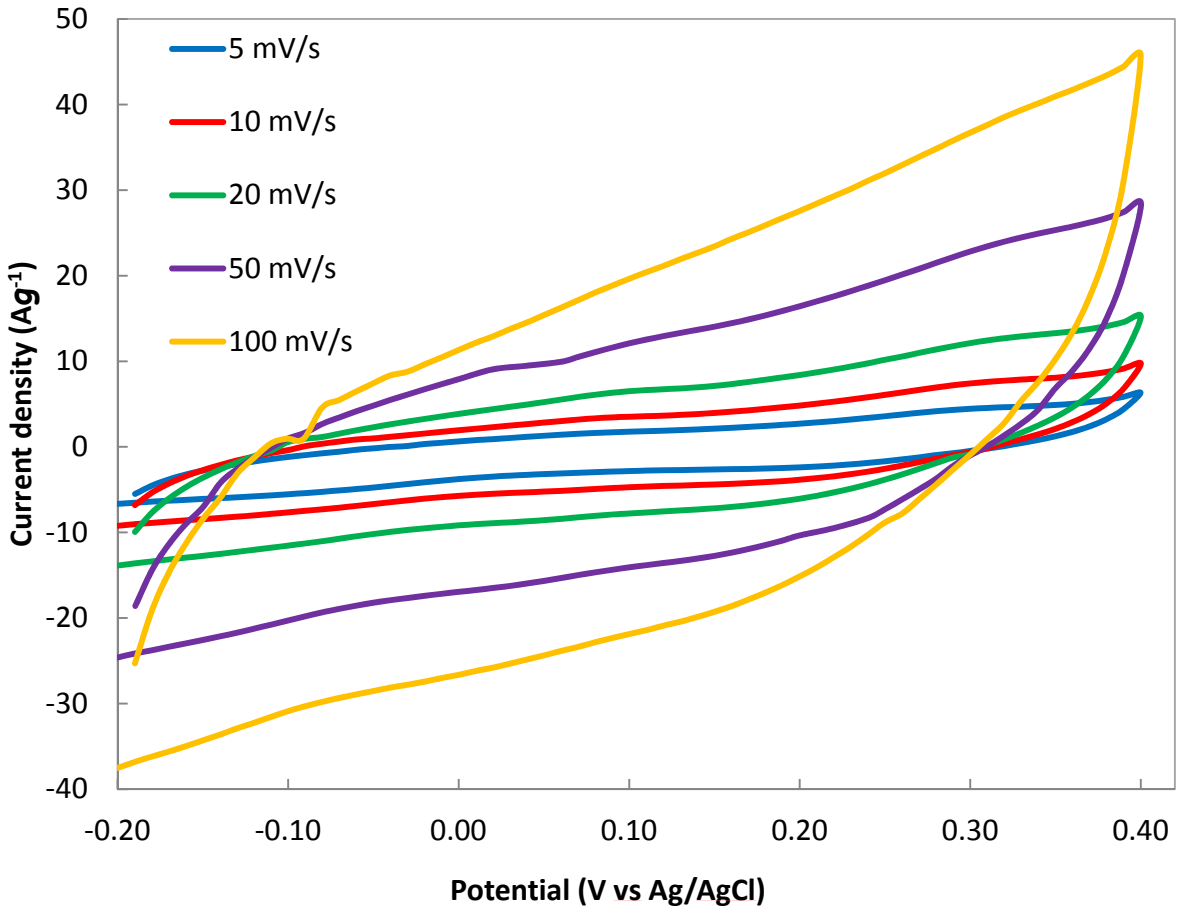
5 mV/s
10 mV/s
20 mV/s
50 mV/s
100 mV/s
Current density (Ag-1)
Potential (V vs Ag/AgCl)
50
40
30
20
10
0
-10
-20
-30
-40
-0.20
-0.10
0.00
0.10
0.20
0.30
0.40

Figure 4b.

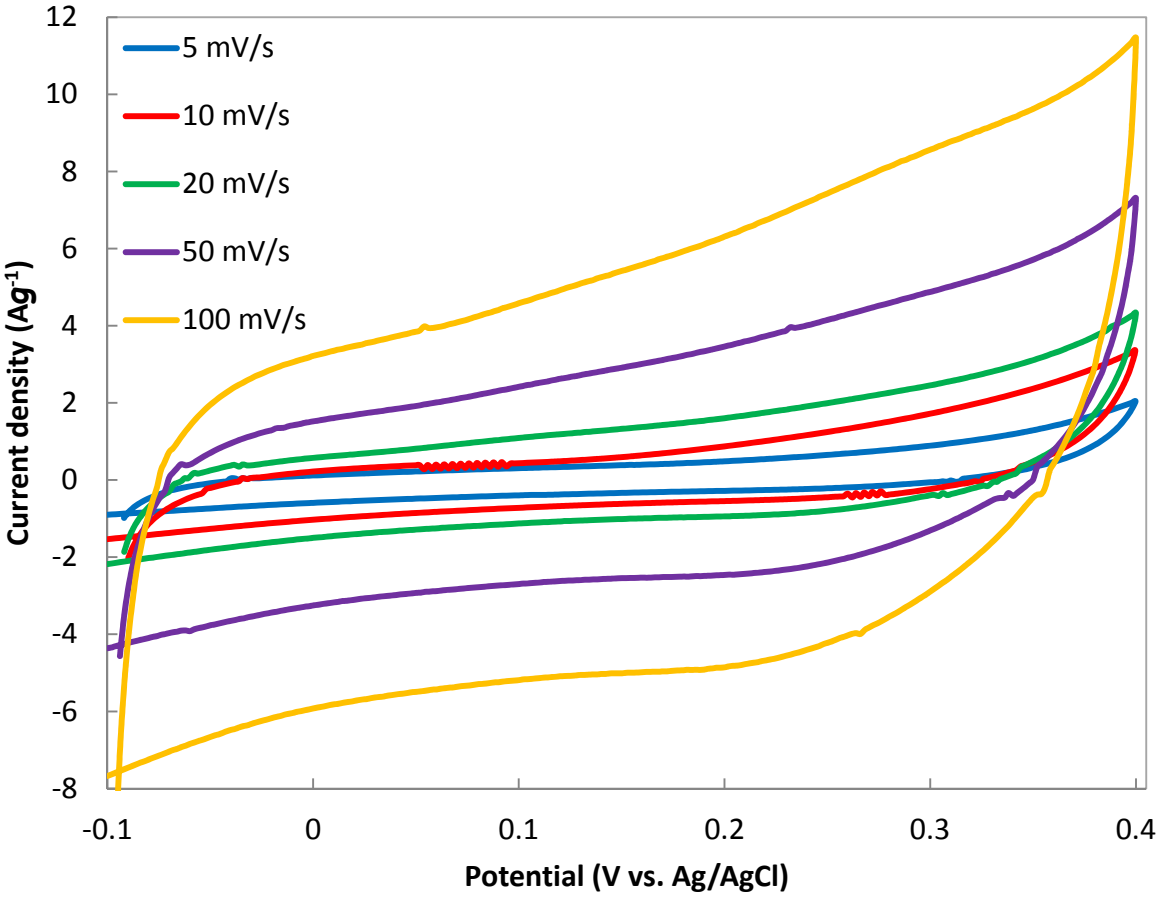
5 mV/s
10 mV/s
20 mV/s
50 mV/s
100 mV/s
Current density (Ag-1)
Potential (V vs. Ag/AgCl)
12
10
8
6
4
2
0
-2
-4
-6
-8
-0.1
0
0.1
0.2
0.3
0.4

Figure 4c.

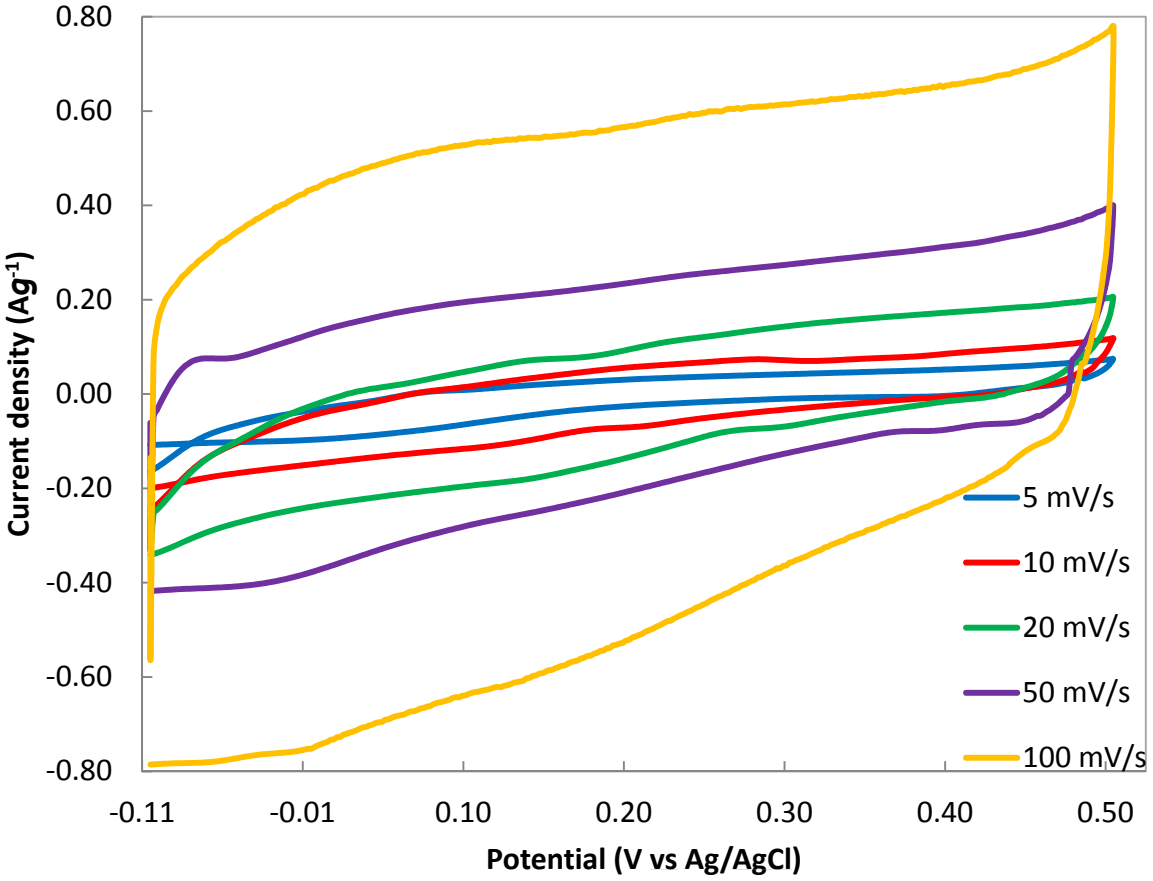
0.80
0.60
0.40
0.20
0.00
-0.20
-0.40
-0.60
-0.80
Current density (Ag-1)
-0.11
-0.01
0.10
0.20
0.30
0.40
0.50
Potential (V vs Ag/AgCl)
5 mV/s
10 mV/s
20 mV/s
50 mV/s
100 mV/s

Figure 4d.

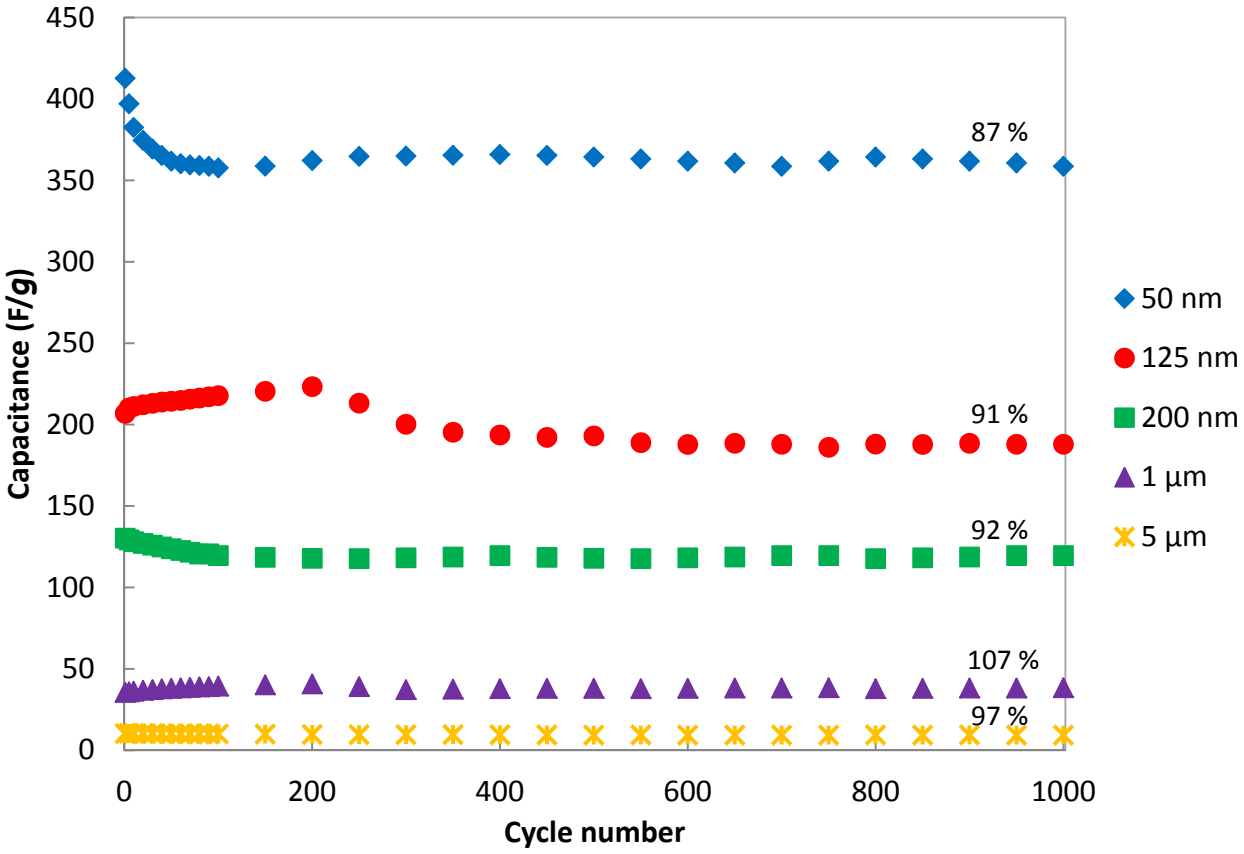
450
400
350
300
250
200
150
100
50
0
Capacitance (F/g)
0
200
400
600
800
1000
Cycle number
87 %
91 %
92 %
107 %
97 %
50 nm
125 nm
200 nm
1 µm
5 µm

Figure 5a.

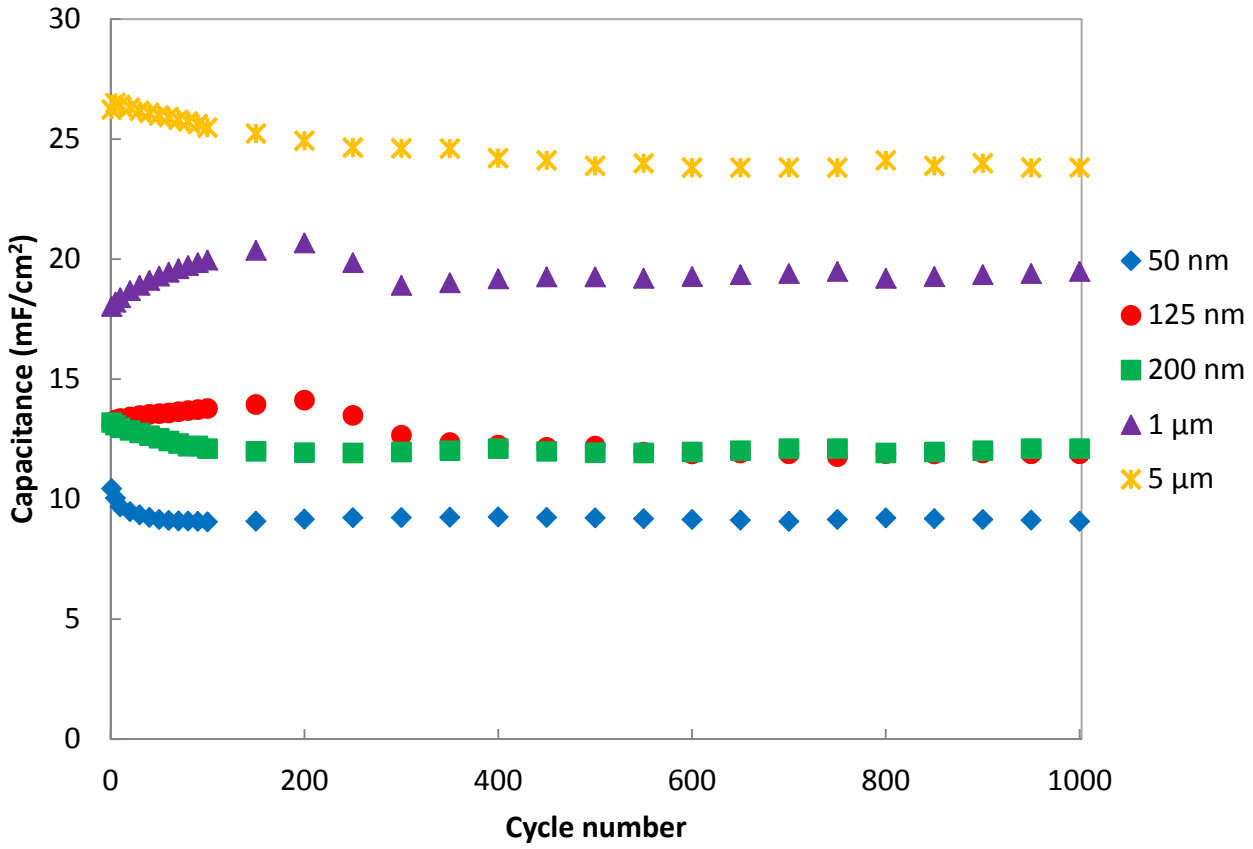
30
25
20
15
10
5
0
Capacitance (mF/cm²)
0
200
400
600
800
1000
Cycle number
50 nm
125 nm
200 nm
1 µm
5 µm

Figure 5b.

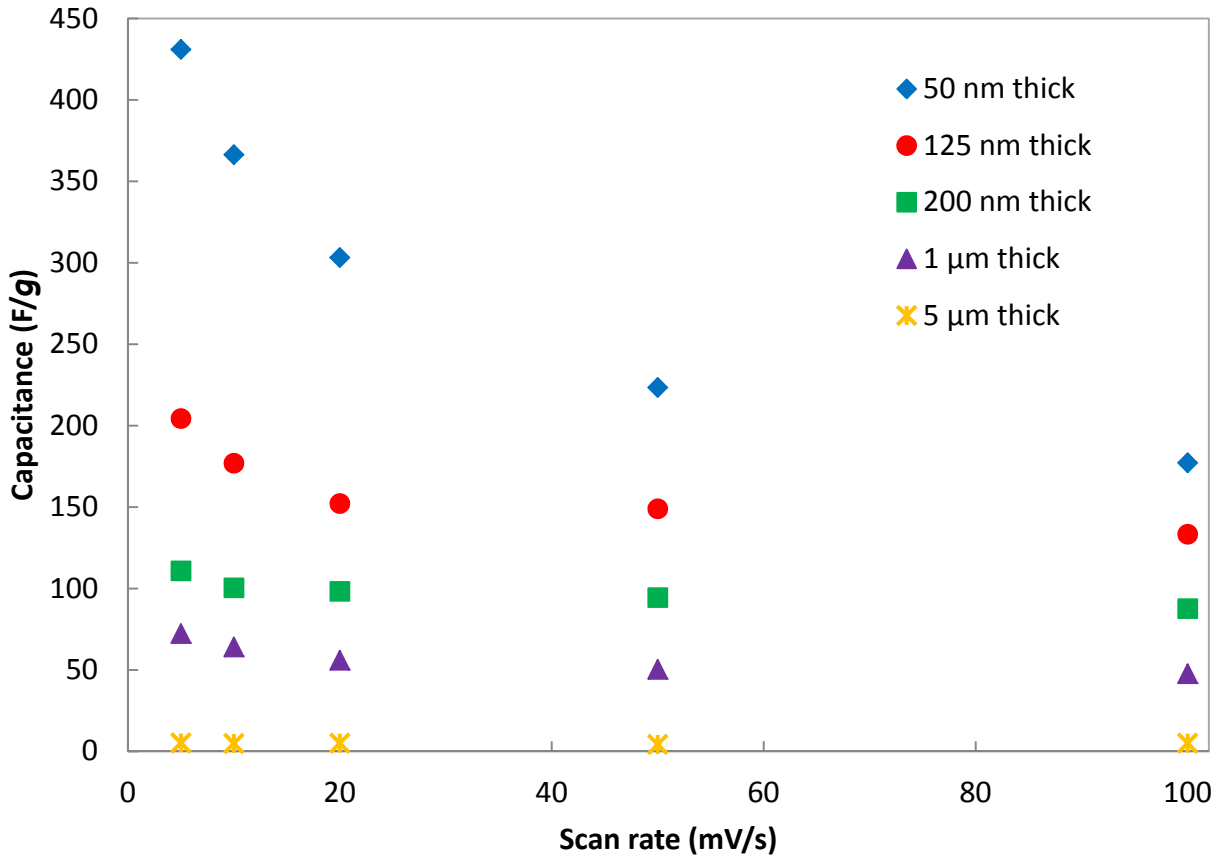
450
400
350
300
250
200
150
100
50
0
Capacitance (F/g)
0
20
40
60
80
100
Scan rate (mV/s)
50 nm thick
125 nm thick
200 nm thick
1 µm thick
5 µm thick

Figure 6.

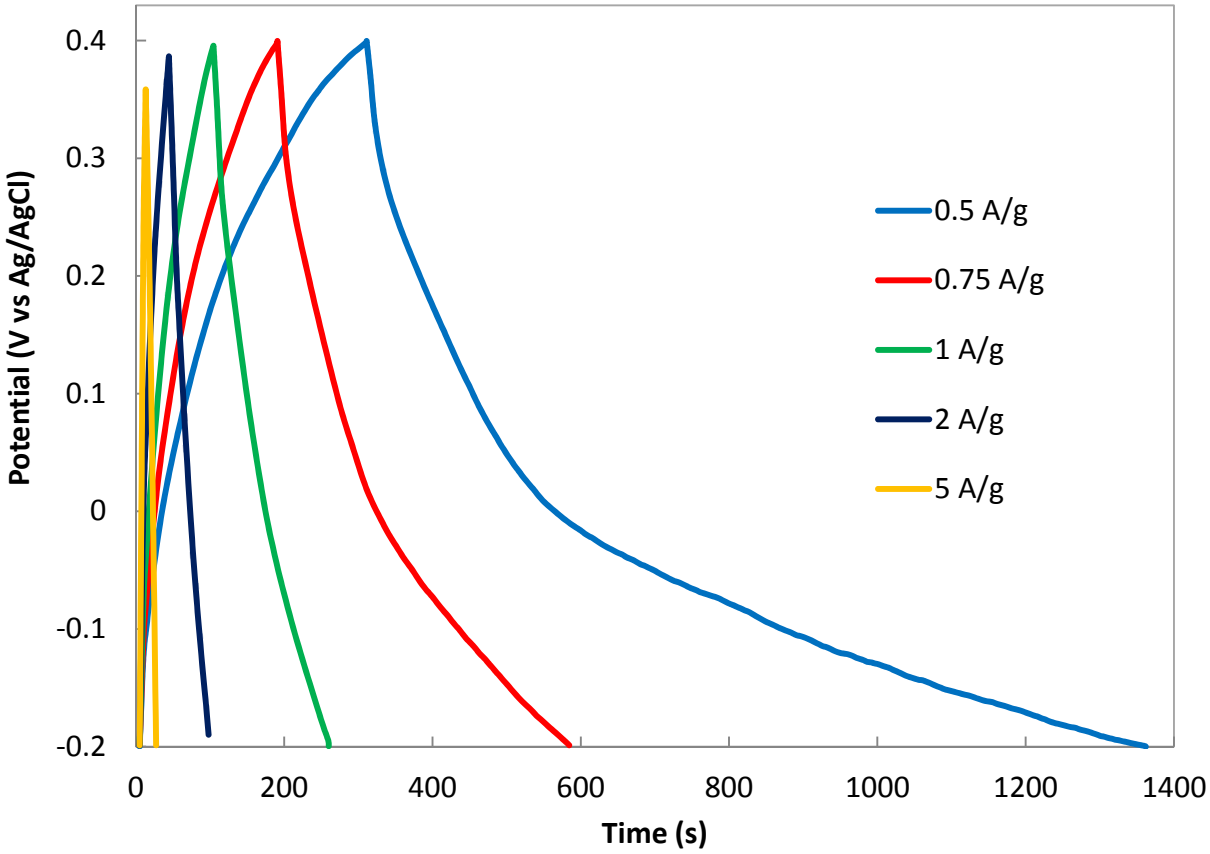
0.4
0.3
0.2
0.1
0
-0.1
-0.2
Potential (V vs Ag/AgCl)
0
200
400
600
800
1000
1200
1400
Time (s)
0.5 A/g
0.75 A/g
1 A/g
2 A/g
5 A/g

Figure 7a.

500

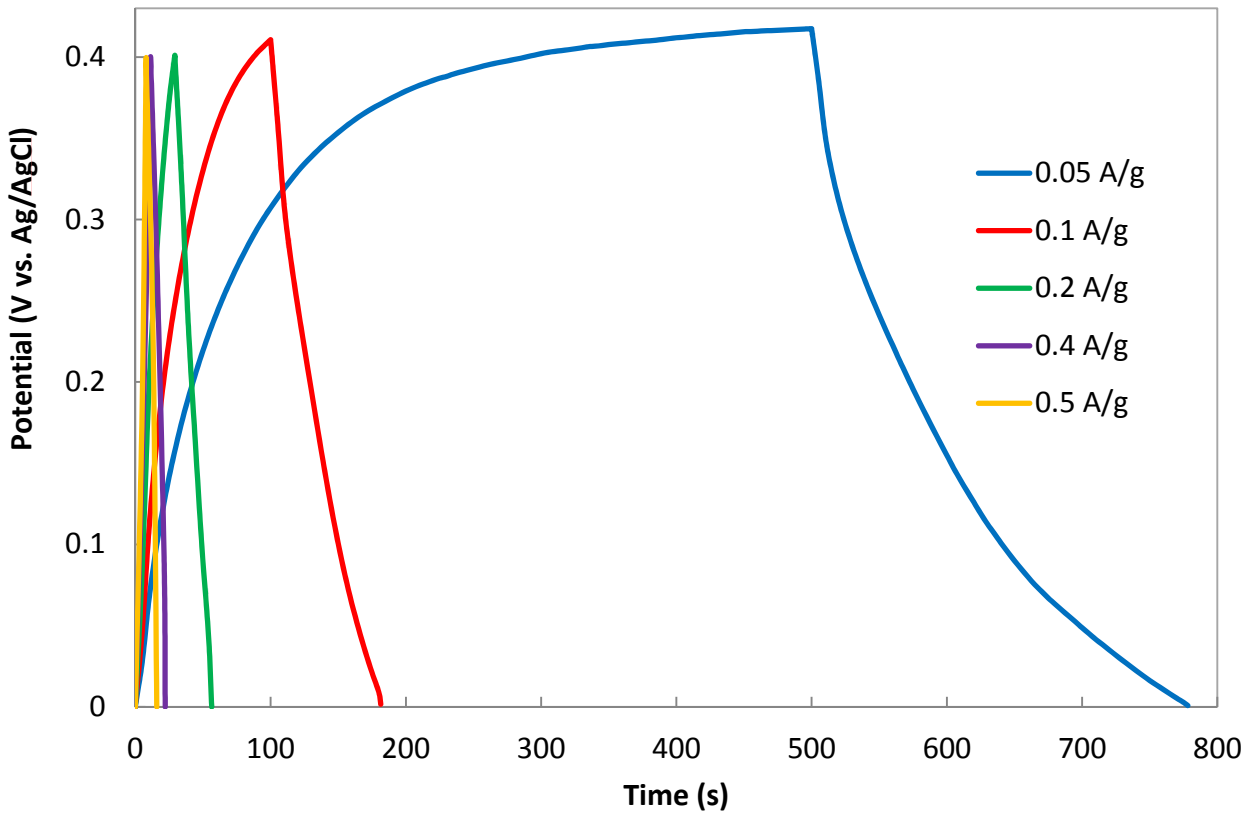

501

502 Figure 7b

503

504

505

506

507

508

509

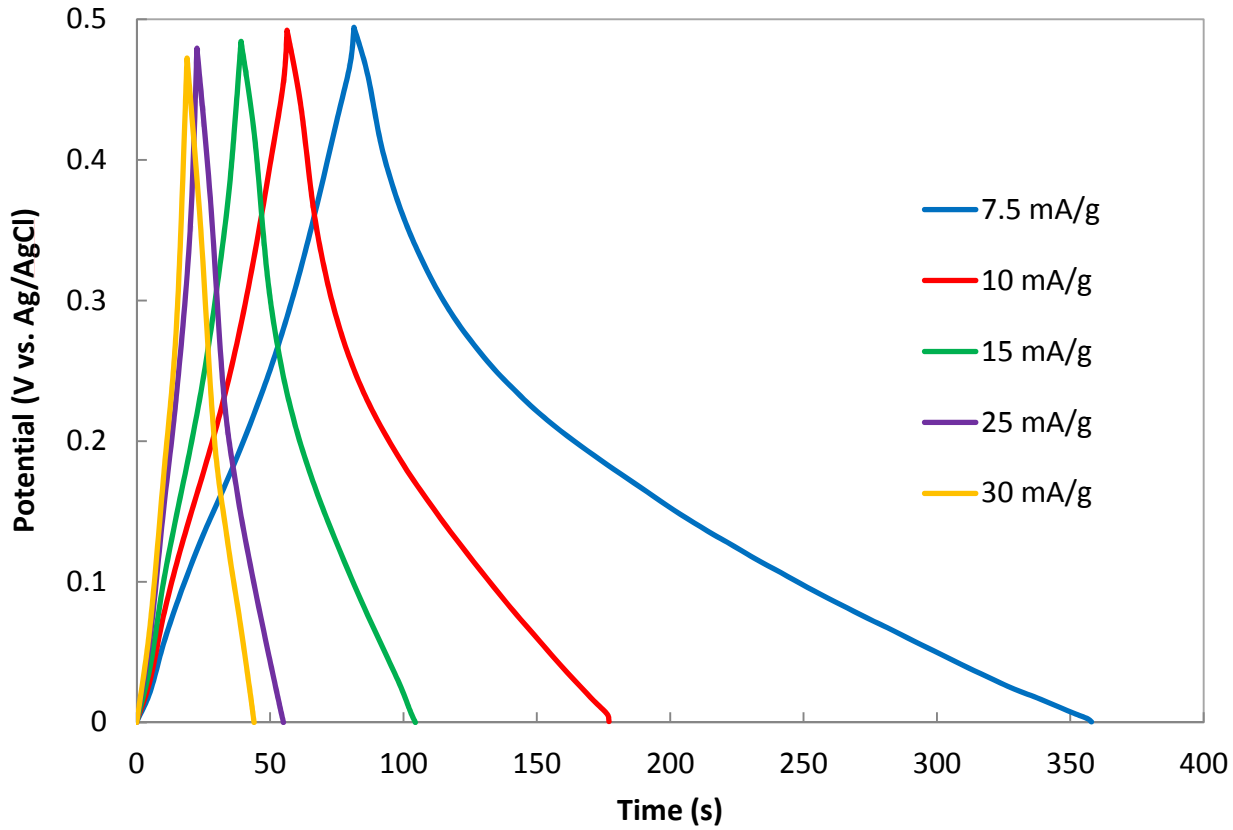
0.5
0.4
0.3
0.2
0.1
0
Potential (V vs. Ag/AgCl)
0
50
100
150
200
250
300
350
400
Time (s)
7.5 mA/g
10 mA/g
15 mA/g
25 mA/g
30 mA/g

Figure 7c

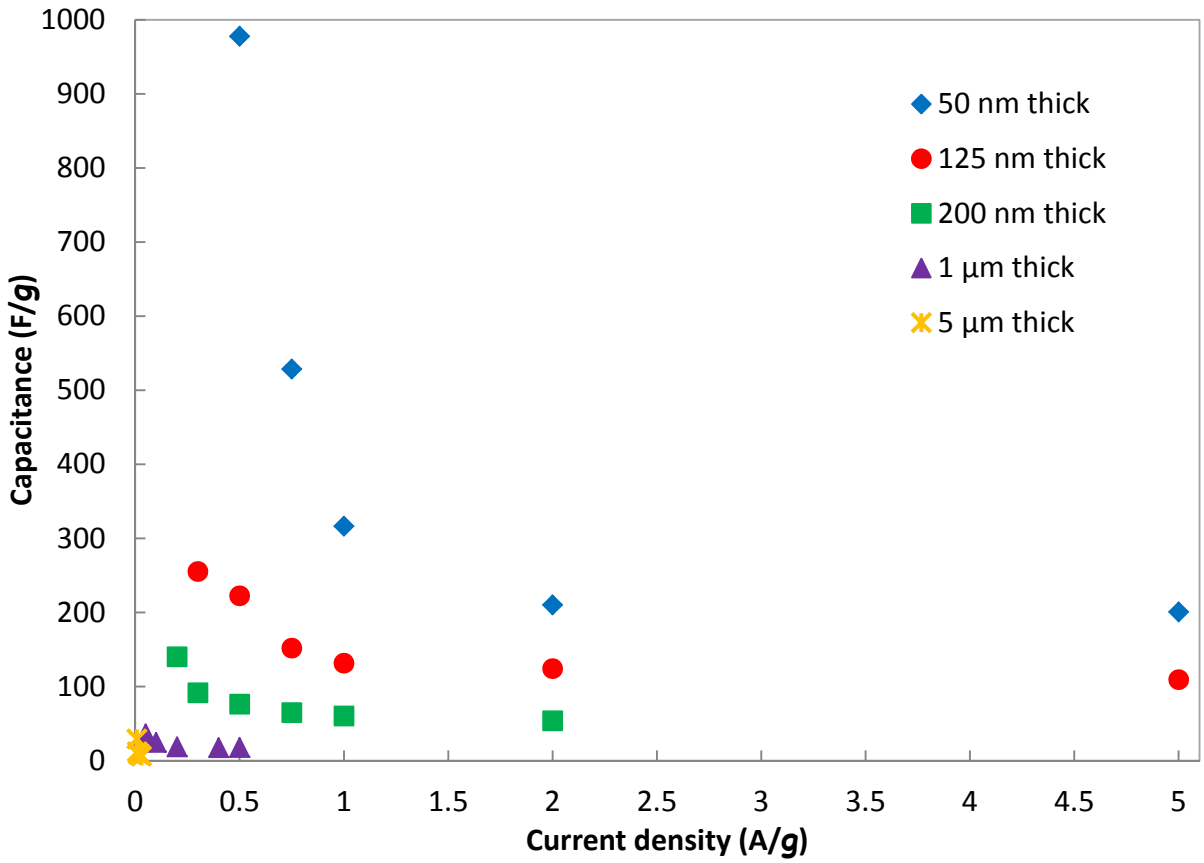
1000
900
800
700
600
500
400
300
200
100
0
Capacitance (F/g)
0
0.5
1
1.5
2
2.5
3
3.5
4
4.5
5
Current density (A/g)
50 nm thick
125 nm thick
200 nm thick
1 µm thick
5 µm thick

Figure 8.

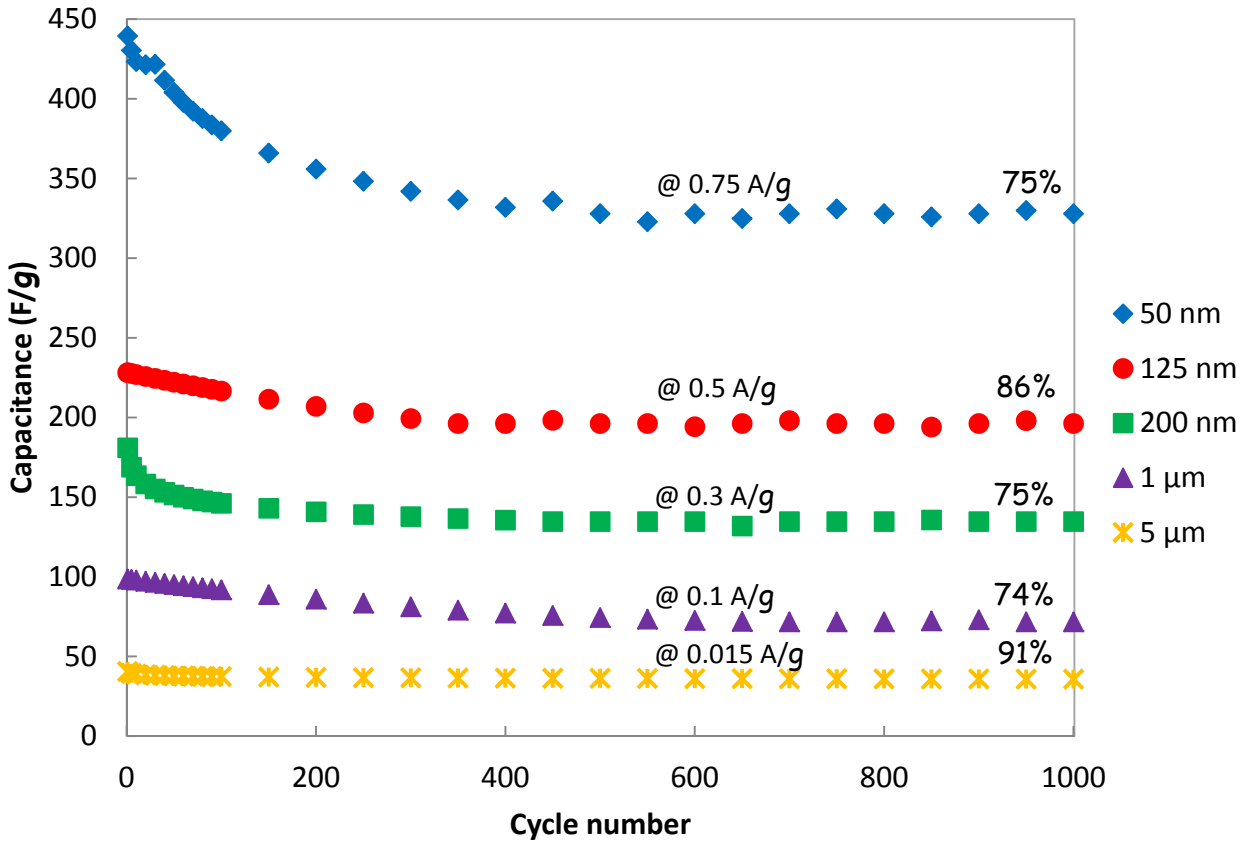
450
400
350
300
250
200
150
100
50
0
Capacitance (F/g)
0
200
400
600
800
1000
Cycle number
@ 0.75 A/g
75%
@ 0.5 A/g
86%
@ 0.3 A/g
75%
@ 0.1 A/g
74%
@ 0.015 A/g
91%
50 nm
125 nm
200 nm
1 µm
5 µm

Figure 9.

543

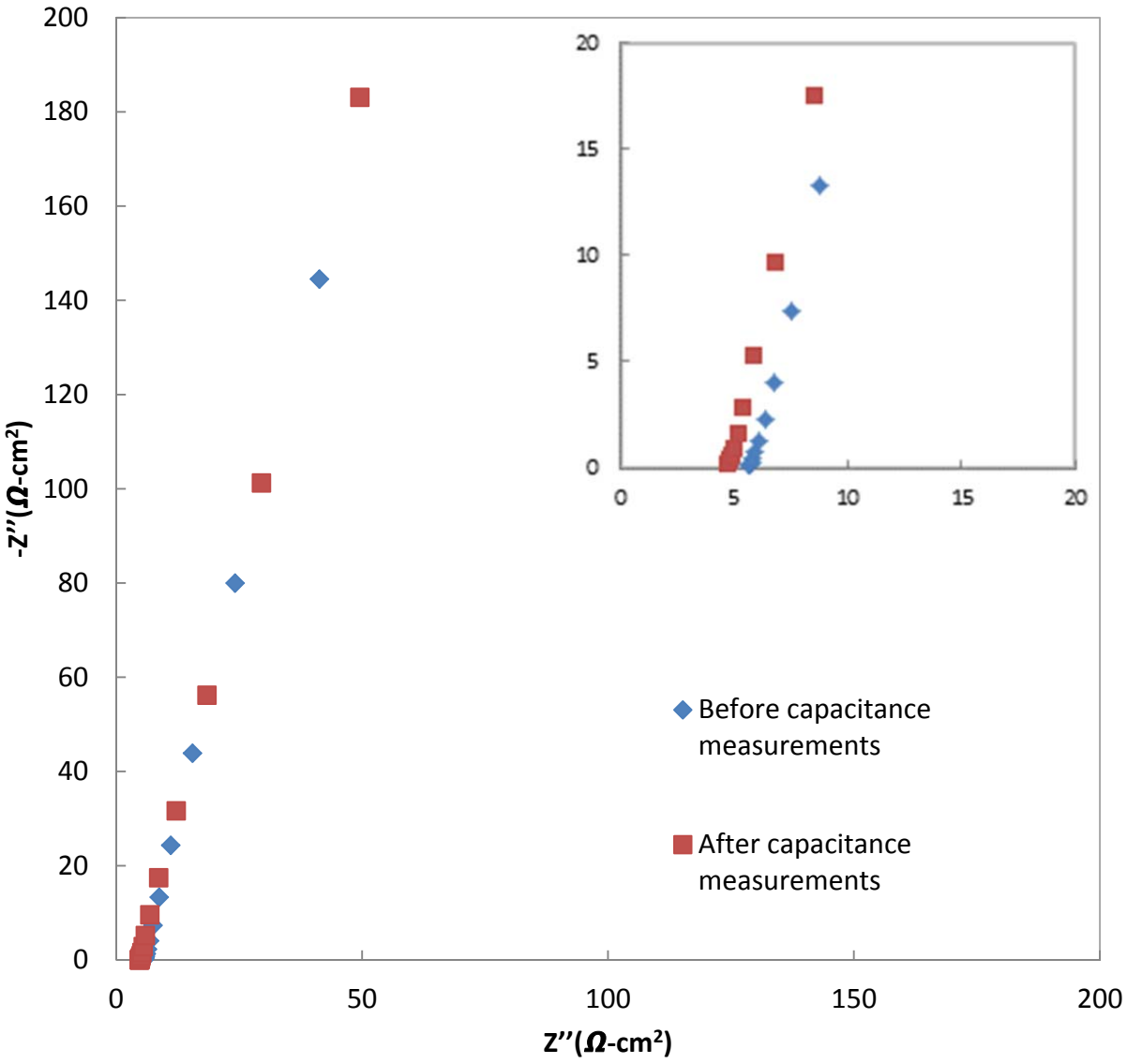

544

545

546 Figure 10.

547

548